

A Single Mms2 “Key” Residue Insertion into a Ubc13 Pocket Determines the Interface Specificity of a Human Lys⁶³ Ubiquitin Conjugation Complex[§]

Received for publication, September 13, 2004, and in revised form, February 10, 2005
Published, JBC Papers in Press, March 4, 2005, DOI 10.1074/jbc.M410469200

Landon Pastushok^{‡§}, Trevor F. Moraes^{¶||}, Michael J. Ellison^{¶**}, and Wei Xiao^{‡ ††}

From the [‡]Department of Microbiology and Immunology, University of Saskatchewan, Saskatoon, Saskatchewan S7N 5E5, Canada and [¶]Department of Biochemistry and ^{**}Institute for Biomolecular Design, University of Alberta, Edmonton, Alberta T6G 2H7, Canada

Human Ubc13 and Mms2 (or its homolog, Uev1) form a unique ubiquitin-conjugating enzyme (Ubc) complex that generates atypical Lys⁶³-linked ubiquitin conjugates. Such conjugates are attached to specific targets that modulate the activity of various cellular processes including DNA repair, mitotic progression, and nuclear factor- κ B signaling. Whereas Ubc13 is a typical Ubc, Mms2 is a non-catalytic Ubc variant. Substantial biochemical evidence has revealed a mechanism whereby Mms2 properly orients ubiquitin to allow for Lys⁶³ conjugation by Ubc13; however, how this specific Ubc13-Mms2 complex is formed and why Mms2 does not form a complex with other Ubcs have not been reported. In order to address these questions, we used a structure-based approach to design mutations and characterize the human Ubc13-Mms2 interface. We used the yeast two-hybrid assay, glutathione S-transferase pull-downs, and surface plasmon resonance to test *in vivo* and *in vitro* binding. These experiments were paired with functional complementation and ubiquitin conjugation studies to provide *in vivo* and *in vitro* functional data. The results in this study allowed us to identify important residues of the Ubc13-Mms2 interface, determine a correlation between heterodimer formation and function, and conclude why Mms2 forms a specific complex with Ubc13 but not other Ubc proteins.

In recent years, the attachment of ubiquitin (Ub)¹ to its target has become one of the cornerstones of covalent post-translational modification in eukaryotes. The biochemical process, called ubiquitination, is a sequential three-step reaction

* This work was supported in part by Canadian Institutes of Health Research Grant MOP-53240 (to W. X.). The costs of publication of this article were defrayed in part by the payment of page charges. This article must therefore be hereby marked “advertisement” in accordance with 18 U.S.C. Section 1734 solely to indicate this fact.

[§] The on-line version of this article (available at <http://www.jbc.org>) contains supplemental Figs. S1–S3.

[¶] A Natural Sciences and Engineering Research Council of Canada Scholar.

^{||} A Canadian Institutes of Health Research Scholar.

^{††} To whom correspondence should be addressed: Dept. of Microbiology and Immunology, University of Saskatchewan, 107 Wiggins Rd., Saskatoon, Saskatchewan S7N 5E5, Canada. Tel.: 306-966-4308; Fax: 306-966-4311; E-mail: wei.xiao@usask.ca.

¹ The abbreviations used are: Ub, ubiquitin; Ubc, ubiquitin-conjugating enzyme; E2, ubiquitin carrier protein; Uev, ubiquitin-conjugating enzyme variant; E3, ubiquitin-protein isopeptide ligase; SPR, surface plasmon resonance; MMS, methylmethane sulfonate; GST, glutathione S-transferase; PBS, phosphate-buffered saline; SD, synthetic dextrose; YPD, yeast extract-peptone-dextrose; RU, response unit(s); RUeq, response unit(s) at equilibrium.

whereby Ub is activated in an ATP-dependent manner by a ubiquitin-activating enzyme. The Ub C terminus then forms a thiolester intermediate with the catalytic Cys residue of a Ub-conjugating enzyme (Ubc or E2) active site. The final step involves a substrate-specific ubiquitin ligase (E3) and leads to the attachment of the Ub C terminus to an ϵ -amino group of a Lys residue of the target (reviewed in Ref. 1). Most often, the process is repeated, and subsequent Ub molecules are attached to one another so that poly-Ub chains are generated. Mono-Ub or poly-Ub chains are used as signals for numerous cellular processes such as cell cycle progression (2), apoptosis (3), mitochondrial inheritance (4), and transcriptional regulation (5).

The versatility of ubiquitination and its ability to function in a wide variety of cellular roles are generally attributed to three main factors. First, whereas E1s are encoded by one or very few genes in the cell, E2s are a more plentiful family, with 13 such enzymes in budding yeast and many more in higher eukaryotes. Second, the most plentiful and diverse group of ubiquitination enzymes is the E3s, which function alone or as part of multi-subunit complexes. E3s are responsible for determining substrate specificity and act in either active or passive roles in ubiquitination by covalently binding Ub or acting as E2 substrate adapter proteins, respectively. A third important factor in providing versatility for ubiquitination involves the nature of the poly-Ub chains themselves.

Conventional poly-Ub chains are built via Lys⁴⁸ and provide a characteristic signal for substrate-specific degradation by the 26S proteasome (6). Because protein turnover by the Ub proteasome system is a fundamental process, it is not surprising that Lys⁴⁸ poly-Ub chains play such a pivotal role in the cell. However, because Ub has six other surface Lys residues, an even greater level of versatility is possible. Indeed, several studies have reported non-standard poly-Ub chains via the Lys⁶ (7), Lys²⁹ (8), Lys¹¹ (9), and Lys⁶³ (10) residues of Ub. Furthermore, such atypical conjugates have been shown to function in roles other than proteasome degradation. Some of the best-documented examples of such poly-Ub chains involve those through Lys⁶³, which have been demonstrated in a stress response (8), mitochondrial inheritance (4), plasma membrane protein endocytosis (11), ribosome function (10), and DNA post-replication repair (12).

Because all Ubcs, regardless of the poly-Ub chain synthesized, have a well-conserved core domain that houses the active site (13), part of the allure in studying atypical Ub chains lies in how they are assembled. The only example to date came as a breakthrough in the field when it was discovered that conjugation via Lys⁶³ occurred through a novel mechanism requiring a heterodimeric complex between Ubc13 and a Ubc enzyme variant (Uev), Mms2 (12). Uev proteins are similar in second-

ary and tertiary structure to E2s, but they lack the catalytic active site that forms thioesters with Ub. Thus, it was originally proposed that the *UEVs* might act as dominant-negative regulators of ubiquitination (14); however, subsequent studies revealed otherwise. *UBC13*, *MMS2*, and Lys⁶³ poly-Ub chains were shown to be indispensable for promoting postreplication repair (12).

Spurred by the uniqueness of E2-Uev-mediated catalysis of Lys⁶³ Ub chains, the crystal structures for the human (15) and yeast (16) Ubc13-Mms2 complexes were solved; both structures were highly superimposable, and each study proposed a similar means for chain catalysis. The three-dimensional studies were followed by extensive NMR analyses that revealed the unique mechanistic basis behind Lys⁶³ poly-Ub chain catalysis. Briefly, a T-shaped heterodimer is formed that allows Mms2 to orient an acceptor Ub through non-covalent contacts such that its Lys⁶³ residue is presented to the donor Ub at the Ubc13 active site. An isopeptide bond can then form between the two molecules, and Lys⁶³ di-Ub is free to exit through a channel leading from the Ubc13 active site toward a E3 binding site (17–20).

The revelation of Ubc13-Mms2-mediated catalysis suggested the necessity of heterodimer formation between the E2 and Uev; however, studies to date have not addressed in detail the significance of the Ubc13-Uev interface. Therefore, we carried out studies using structural information and a site-directed mutagenesis approach to provide a dedicated structure-function study of the human Ubc13-Mms2 interface. In our rational approach, the goals were as follows: 1) to identify key residues in Ubc13 and Mms2 that are important for complex formation; 2) to demonstrate a correlation between Ubc13-Mms2 interaction and function; and 3) to determine why Mms2 forms a specific complex with Ubc13, and not other Ubc.

EXPERIMENTAL PROCEDURES

Strains and Cell Culture—*Saccharomyces cerevisiae* haploid strains used in this study include PJ69-4A (*MATa trp1-901 leu2-3, 112 ura3-52 his3-200 gal4Δ gal80Δ P_{GAL2}-ADE2 LYS2::P_{GAL1}-HIS3 met2::P_{GAL1}-lacZ*, a gift from Dr. P. James (University of Wisconsin, Madison, WI). A wild-type haploid *S. cerevisiae* strain HK580-10D (*MATa ade-1 can1-100 his3-11,15 leu2-3, 112 trp1-1 ura3-1*) was received from Dr. H. Klein (New York University) and used as the recipient to delete the entire *MMS2* open reading frame by a one-step gene replacement method (21) using an *mms2Δ::HIS3* cassette generated through PCR amplification as previously described (22). A *ubc13Δ* HK580-10D strain was created with the same approach, using a *ubc13Δ::HIS3* cassette (23). Yeast cells were cultured at 30 °C either in a complete yeast extract-peptone-dextrose (YPD) medium or in a synthetic dextrose (SD) medium supplemented with necessary nutrients as recommended (24). To make plates, 2% agar was added to either YPD or SD medium prior to autoclaving. Yeast cells were transformed using a dimethyl sulfoxide-enhanced LiAc method as described previously (25). Bacterial strains used in this study include BL21(DE3)-RIL (Stratagene), an *Epicurian coli* strain that contains extra copies of the *argU*, *ileY*, and *leuW* tRNA genes to facilitate recombinant protein expression. *Escherichia coli* DH10B was used for DNA plasmid propagation and isolation. Bacterial cells containing plasmids were cultured at 37 °C in LB supplemented with ampicillin to a final concentration of 50 μg/ml.

Plasmids—The human *UBC13* open reading frame was PCR-amplified as an EcoRI-SalI fragment and cloned into pGBT9 (purchased from Clontech) to form pGBT-hUBC13, an N-terminal fusion to Gal4_{BD}. The same *UBC13* fragment was similarly cloned into pGEX6 (purchased from Amersham Biosciences) to form an N-terminal gene fusion to glutathione *S*-transferase (GST) and named pGEX-hUBC13. Human *MMS2* cDNAs were isolated as previously reported (26). The open reading frame was PCR-amplified as a BamHI-SalI fragment and cloned into pGAD424 (Clontech) to form an N-terminal fusion to GAL4_{AD}, named pGAD-hMMS2. The same *MMS2* fragment was cloned into pGEX6 to form an N-terminal fusion to GST, named pGEX-hMMS2. Yeast two-hybrid or GST fusion plasmids containing site-specific mutations within *hUBC13* or *hMMS2* were constructed by the mega-primer approach (27).

Recombinant Protein Expression and Purification—BL21(DE3)-RIL cells transformed with pGEX6-hMMS2 or pGEX-hUBC13 were grown overnight at 37 °C in LB supplemented with ampicillin and then subcultured 1:10 the following day. Cells were grown to an A₆₀₀ of 0.6 and induced with isopropyl-β-D-thiogalactopyranoside (0.5 mM) for 3 h. Cells were harvested by centrifugation at 5000 rpm and resuspended in phosphate-buffered saline (PBS) (140 mM NaCl, 2.7 mM KCl, 10 mM Na₂HPO₄, and 1.8 mM KH₂PO₄, pH 7.3). Crude extracts were generated after cell lysis by French Press at 10,000 p.s.i., and the soluble fraction was retained after centrifugation at 30,000 rpm. All subsequent steps were performed at 4 °C. Soluble extracts were passed through a pre-packed 5-ml GStrap column (Amersham Biosciences), which was then washed with 5 column volumes of 1× PBS. GST fusion proteins were eluted with reduced glutathione elution buffer (10 mM glutathione in 50 mM Tris-HCl, pH 8.0) and dialyzed extensively against cleavage buffer (50 mM Tris-HCl, 150 mM NaCl, 1 mM EDTA, and 1 mM dithiothreitol, pH 7.0). When needed, cleavage was achieved after the addition of 2 units of Precission™ Protease per mg of fusion protein with a 16-h incubation and gentle rocking. Cleaved proteins were then applied to a GStrap column in order to remove the GST component from hMms2 or hUbc13. Protein concentrations were determined using the BCA™ Protein Assay Kit (Pierce) as per the instruction manual.

GST Pull-downs—GST pull-downs were performed using MicroSpin GST Purification Modules (Amersham Biosciences). 0.03 mg of purified GST fusion protein in 1× PBS was loaded and incubated in the purification module for 1 h at 4 °C with gentle rocking. The module was then washed three times with 500 μl of PBS. Subsequently, 0.03 mg of purified, non-fused hUbc13 or hMms2 in 1× PBS was added to the module, and the incubation was continued for another hour at 4 °C. The module was washed again three times with 500 μl of PBS, and then 80 μl of reduced glutathione elution buffer was added to elute the affinity-purified proteins. Eluted samples were subjected to 12% SDS-PAGE and Western analysis.

Yeast Two-hybrid Analysis—The yeast two-hybrid strain PJ69-4A (28) was co-transformed with different combinations of Gal4_{BD} and Gal4_{AD} constructs. The co-transformed colonies were initially selected on SD-Trp-Leu. For each transformation, at least four independent colonies were grown in SD-Trp-Leu media, and then plated as replicates onto SD-Trp-Leu-His + 3-aminotriazole to test the activation of the *P_{GAL1}-HIS3* gene.

Functional Complementation of Yeast Mutations by Human Genes—The gradient plate assay was performed as a semiquantitative measurement of relative MMS sensitivity. The HK580-10D *mms2Δ* or *ubc13Δ* strains were transformed with pGAD-hMMS2 or pGBT-UBC13 two-hybrid plasmid, respectively. At least three individual transformants were each inoculated into 1 ml of SD minimal media to select for overnight cultures containing the plasmids. To prepare the plates, molten YPD agar (30 ml) was mixed with the appropriate concentration of MMS to form a bottom layer. The gradient was created by pouring this layer into tilted square Petri dishes. After solidification for 1 h, the Petri dishes were returned flat, and 30 ml of the same molten agar without MMS was poured to form the top layer. Cells (0.1 ml) were taken from an overnight culture, mixed with 0.4 ml of sterile water and 0.5 ml of 2% molten YPD agar, and then immediately imprinted onto freshly made gradient plates via a microscope slide.

Surface Plasmon Resonance—SPR was performed using a Biacore X instrument. To create a chip for protein interaction analysis, a research-grade CM5 sensor chip was used to immobilize anti-GST antibody by amine coupling, according to instructions in the Amine Coupling and GST Capture Kits (Biacore). Approximately 15,000 response units (RU) of anti-GST antibody was immobilized to each of the two flow cells (Fc1 and Fc2). For all SPR experiments, GST fusion or native proteins were purified to >95% homogeneity and dialyzed against HBS buffer (50 mM HEPES, 150 mM NaCl, 3 mM EDTA, and 0.005% Surfactant P20, pH 7.5). A flow rate of 20 μl/min and a 2-min injection of 5 μg/ml protein was used to capture ~1000 RU of the GST fusion protein (ligand) in Fc2. For a control, purified recombinant GST (GST Capture Kit; Biacore) was similarly injected into the other flow cell to capture ~1000 RU in Fc1. All data generated were corrected for background in real time (Fc2 – Fc1). 10 μl of the soluble protein (analyte) at various concentrations was then applied to the flow cells at 5 μl/min for 2 min to yield binding curves. Regeneration of the sensor chip surface was accomplished with a 20 μl/min injection of 10 mM glycine, pH 2.2, for 2 min. For binding constant determination, Biacore BiaEvaluations software was used to fit curves (1:1 molecular binding with mass transport) generated from free analyte concentrations ranging from 1 × 10⁻⁸ to 5 × 10⁻⁸ M for Mms2 and from 2.5 × 10⁻⁸ to 5 × 10⁻⁷ M for Ubc13. The χ² values were 5.2 and 2.3 for GST-Mms2 binding Ubc13 and GST-

Ubc13 binding Mms2, respectively. The data are deemed reliable if χ^2 is <10 . To confirm the reliability of the data, we generated plots of the response (RU) versus free analyte (nM) and calculated the K_d , where $K_d = \text{RU}_{\text{max}} \times \text{slope}$ in the double reciprocal plot (1/response versus 1/free analyte).

In Vitro Ubiquitination Assay—A 0.5-ml conjugation reaction containing Uba1 (20 nM), ^{35}S -labeled Ub (2.5 μM), and Ubc13 or Mms2 (250 nM) in an ATP mixture (10 mM HEPES, pH 7.5, 5 mM MgCl_2 , 5 mM ATP, and 0.6 unit/ml inorganic phosphatase) was incubated at 30 °C for 60 min. The concentration of each component is noted in the figure legends. Reactions were terminated by the addition of trichloroacetic acid to a final concentration of 10% and processed for SDS-PAGE and subsequent analysis by autoradiography.

RESULTS

The Ubc13-Mms2 Structure—The overall structure of the human Ubc13-Mms2 heterodimer is shown in Fig. 1A. Each molecule adopts the characteristic α/β Ubc fold (for example, see Refs. 13 and 29) and exhibits a very similar three-dimensional structure, with the main exception that Mms2 lacks two C-terminal α -helices. The N terminus, $\alpha 1$ helix, and the Loop 1 portions of Mms2 pack against Ubc13 to form a unique end-on structure that creates a long channel which buries ~ 1500 Å of solvent-accessible surface area (15, 16).

Fig. 1B is oriented similarly to Fig. 1A and reveals the residues in close proximity to the interface. Several factors were important in determining which residues to mutate. First, our early studies on heterodimer formation (17) indicate that the Ubc13-Mms2 complex is stable in salt concentrations of >1 M and therefore suggest a large portion of hydrophobic contacts. Visible inspection reveals that a significant contribution of these hydrophobic contacts likely surround a region that corresponds to a two-residue insertion (Asn¹² and Phe¹³) near the amino end of the $\alpha 1$ helix that is unique to Uev sequences. Second, we previously identified a remarkable change in the orientation of the human Mms2 N terminus upon heterodimer formation with Ubc13 (15), implicating an importance for the Ubc13 residues in proximity to the Mms2 N terminus. Last, each of the residues that we mutated is either completely conserved or very similar when comparing protein sequence alignments across various model organisms (Fig. 1C). The panel of residues that were eventually mutated in these studies is indicated in Fig. 1, B and C.

Design of Ubc13 Mutants and Their Interaction in the Yeast Two-hybrid Assay—Because all evidence to date suggests a specific complex between Mms2 and a single Ubc (namely, Ubc13), we decided to initiate our mutagenesis studies with focus on Ubc13 residues. It was anticipated that this approach would narrow down the search for key residues because Ubc13 involved in very different cellular roles still have very conserved core domain sequences.

As a precursor to selecting mutants to test *in vivo*, we were first able to screen two Ala substitutions, Ubc13-Y34A and Ubc13-L83A, *in vitro* by using the GST pull-down approach as discussed later. These residues had been suggested previously (15) to contribute hydrophobic contacts to two separate regions of the interface (see Fig. 1B). However, neither mutation had a significant effect on binding to Mms2 as determined by GST pull-down and isothermal titration calorimetry experiments,² suggesting that residues presumed to contribute hydrophobic contacts have to be changed more drastically. With this in mind, we targeted another residue of the putative hydrophobic core, Ubc13-Phe⁵⁷, and designed a non-conservative substitution to Glu to introduce a charged polar group into the region.

In another attempt to address this same hydrophobic region, we focused the role of the Ubc13-Glu⁵⁵ residue. Structure anal-

ysis implicates a dual role whereby the β - and γ -carbons of Glu⁵⁵ can provide hydrophobic contacts for Mms2-Phe¹³, whereas its carboxyl group is used to H-bond with Mms2-Asn¹² (15, 16) (Fig. 1B). The only Ubc13 mutant studied to date was of the corresponding Glu⁵⁵ in the yeast Ubc13 (16), for which Ala was substituted, resulting only in a small titration-dependent effect on binding and function (30). Therefore, we created a conservative E55Q mutant that was expected to disrupt the H-bonding with Mms2-Asn¹² while still retaining hydrophobic contacts and approximate size.

The last of our initial Ubc13 mutagenesis focused on Ubc13-Glu⁶⁰, which is situated near the N terminus of Mms2. Although it is not resolved in the human structure, the yeast Ubc13-Mms2 heterodimer shows an H-bond formed between Ubc13-Glu⁶⁰ and Mms2-Ser². It was predicted that a conservative Ubc13-E60Q mutation would disrupt the bond and address the importance of the N terminus of Mms2 in binding Ubc13.

In order to determine the effect of the interface mutations on complex formation in the cell, we first employed the yeast two-hybrid assay as a qualitative measure of interaction strength. Fig. 2 shows the effects of these Ubc13 mutations. The mutation at Glu⁶⁰ (E60Q) does not affect the Ubc13 interaction with Mms2, whereas both E55Q and F57E mutations resulted in the complete disruption of heterodimer formation as visualized in the assay. The severe consequences of the Ubc13-Glu⁵⁵ and Ubc13-Phe⁵⁷ mutants prompted us to investigate another residue in this area, Ubc13-Arg⁷⁰.

The Arg⁷⁰ residue is absolutely conserved among Ubc13s (Fig. 1C). Although it has been suggested that Arg⁷⁰ can provide hydrophobic contacts in the yeast heterodimer structure (16), we note another predominant contribution to the interface as an H-bond with the carbonyl carbon of Mms2-Met⁴¹ (Fig. 1B). To address this bond, we created a Ubc13-R70A mutant and tested its binding to Mms2 in the yeast two-hybrid assay. As seen in Fig. 2, Ubc13-R70A impaired Ubc13-Mms2 interaction.

Design of Mms2 Mutants and Their Interaction in the Yeast Two-hybrid Assay—The finding that all of the Ubc13 residue substitutions that affect binding lie in close proximity allowed us to narrow our search for key interface residues in Mms2. Notably, the Mms2 residues that most closely correspond to these Ubc13 mutants are Mms2-Asn¹² and Mms2-Phe¹³, two amino acids unique to Uevs when aligned against Ubc13 (16).

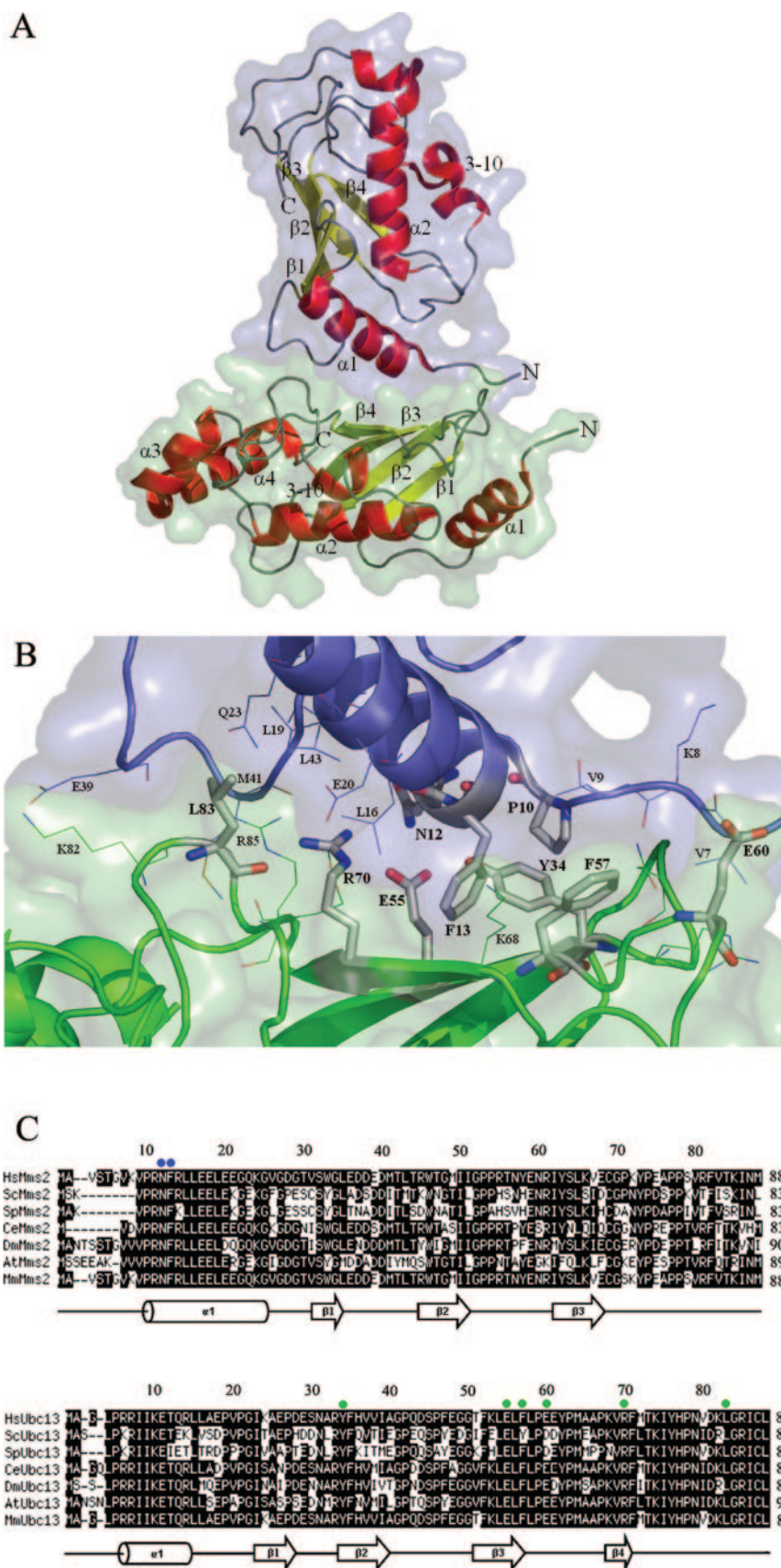
Visualization of the Ubc13-Mms2 heterodimer shows an insertion of the Mms2-Phe¹³ residue into a hydrophobic region, created mainly by the Ubc13 residues mutated above. As with Ubc13-F57E, we decided to exploit this area with an aggressive Mms2-F13E substitution to introduce a polar, charged group to abrogate non-polar contacts.

Unlike Phe¹³, Mms2-Asn¹² does not contribute to the hydrophobic core but instead forms H-bonds with the Ubc13 residues Glu⁵⁵ and Tyr³⁴. However, because only the Ubc13-E55Q mutation showed an effect on binding, we sought to demonstrate a pairwise interaction between it and Mms2-Asn¹². We thus created two Asn¹² mutations, one as a conservative N12D substitution and a second mutation, N12A, in order to abolish any H-bonding possibilities.

When testing these Mms2 mutants in the two-hybrid assay, we found that neither Mms2-N12A nor Mms2-N12D had a detectable effect on inhibiting complex formation as compared with wild-type (Fig. 2). In contrast, the Mms2-F13E mutation seemed to completely disrupt the Ubc13-Mms2 interaction.

Because our mutagenesis of Ubc13 yielded mutants that resulted in severe (Ubc13-E55Q and Ubc13-F57E) and slight (Ubc13-R70A) disruption of the Ubc13-Mms2 interaction, we desired to have a complement of Mms2 mutants with similar

² L. Pastushok, T. F. Moraes, and J. Hu, unpublished data.



effects. Therefore, we hypothesized that because the aggressive introduction of a charged group at Mms2-Phe¹³ (F13E) caused a severe effect on interaction, a more conservative F13Y mutation that simply introduces a small polar hydroxyl group might

cause a moderate effect. Indeed, the Mms2-F13Y mutant did not interact with Ubc13 as strongly as wild-type, but it did not completely abolish heterodimer formation either (Fig. 2).

Taken together, the yeast two-hybrid data indicate that two

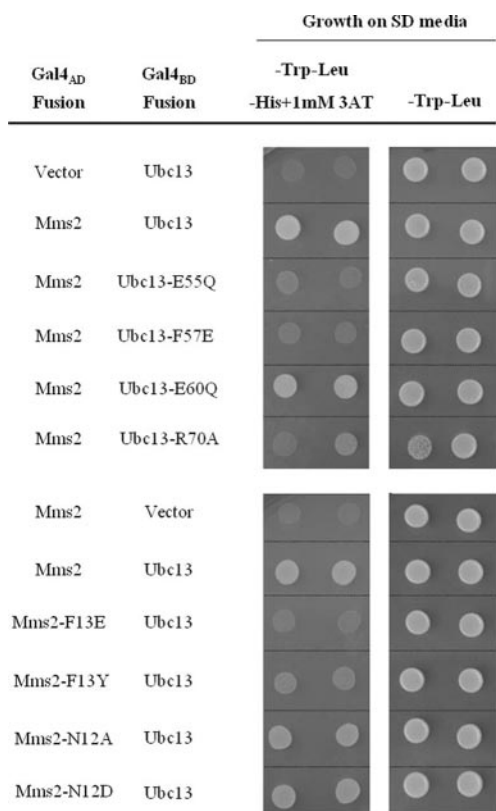


FIG. 2. *In vivo* interaction of mutated Ubc13 and Mms2 with wild-type partners by a yeast two-hybrid assay. Yeast cells transformed with Gal4_{AD} and Gal4_{BD} fusion constructs were used to test the strength of the Ubc13-Mms2 interaction. Association of Ubc13 and Mms2 turns on the *GAL1* promoter, which transcribes the *HIS3* reporter gene. Positive interactions are observed by growth on media without His + 1 mM 3-aminotriazole after 48 h at 30 °C. Plasmids were maintained in the cell by growth on media without Trp and Leu. At least four colonies from each combination were tested, and only two representative colonies are shown. The colony one left of Mms2-Ubc13-R70A did not grow well on nonselective medium and displayed more severe phenotypes than other colonies. Also see Fig. 7A for the phenotype of this combination.

mutants (Mms2-F13Y and Ubc13-R70A) result in weakened interactions between Ubc13 and Mms2. Also, three mutants (Mms2-F13E, Ubc13-E55Q, and Ubc13-F57E) led to the complete disruption of the Ubc13-Mms2 interface. Although it may be argued that some very slight binding might occur below the detectable limits of this assay, we note that the yeast two-hybrid assay is a highly sensitive tool because transient interactions are sufficient to allow transcription of the reporter gene.

The in Vivo Function of MMS2 and UBC13 Mutants Correlates with in Vivo Interaction—MMS2 was first identified by its ability to provide yeast cells with protection from the DNA-damaging agent MMS (31). The discovery revealed the “error-free” (damage avoidance) postreplication repair pathway (reviewed in Ref. 32) that is conserved in human cells (33). Genetically speaking, error-free postreplication repair activity is dependent on *UBC13*, *MMS2*, and Lys⁶³-conjugated poly-Ub chains (12, 20). As a result, *ubc13Δ* and *mms2Δ* are similarly sensitive to DNA damage (23).

Because mammalian *MMS2* (26, 34) and *UBC13* (35) genes are able to functionally complement their yeast counterparts, we decided to test the function of our human interface mutant proteins in the corresponding *ubc13Δ* and *mms2Δ* yeast strains. The approach would verify the correlation between heterodimer formation and function. As seen in Fig. 3, wild-type human *MMS2* and *UBC13* are able to alleviate the MMS sensitivity of their corresponding yeast deletion strains. The

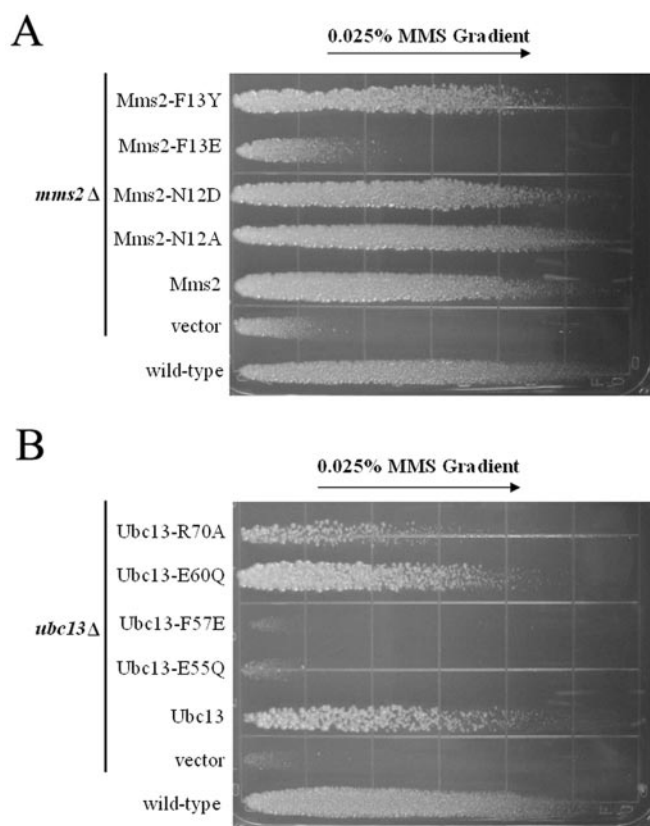


FIG. 3. Functional complementation of yeast *ubc13* and *mms2* mutants by corresponding human genes and their derivatives. The function of human Ubc13 or Mms2 is reflected in the ability to protect its corresponding yeast deletion mutants from killing by MMS. Cells were printed on YPD plates containing 0.025% MMS, and those that survived DNA damage treatment were able to grow further along the gradient. Incubation was carried out for 48 h at 30 °C. All cells grew equally well on YPD plates without MMS (data not shown).

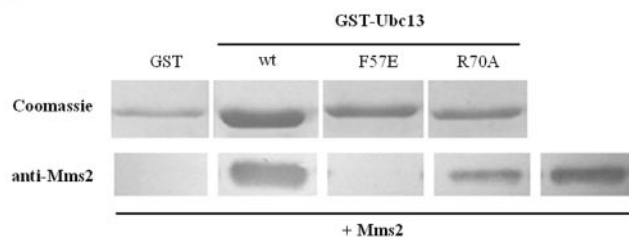
MMS2 mutants at Asn¹² appeared to function as well as wild-type *MMS2*; on the other hand, the mutations at Phe¹³ that address the core hydrophobic region led to a slight (F13Y) or drastic (F13E) reduction in the protection of cells against MMS (Fig. 3A).

As in the two-hybrid assay, the *UBC13* E60Q mutant had no effect on functional complementation (Fig. 3B). However, each of the mutants in proximity to Mms2-Phe¹³ led to compromised Ubc13 function. Most strikingly, both Ubc13-E55Q and Ubc13-F57E mutations had no detectable ability to provide protection against MMS-induced killing when compared with the negative control. The other Ubc13 mutation, R70A, which was designed to destroy H-bonding with the Mms2 backbone, led to a reduced but incomplete loss in the ability to complement the *ubc13* deletion.

The functional experiments above were repeated using UV as a DNA-damaging agent, and we observed no change in the results (data not shown). To account for the heterologous approach, functional complementation was also checked using double transformants (pGBT-hUBC13 and pGAD-hMMS2) in an *mms2Δ ubc13Δ* strain, and our findings were the same (data not shown).

In Vitro Binding of Interface Mutants—The yeast two-hybrid assay provides a good qualitative indication of binding strength; however, several factors such as expression levels and Gal4 fusions can hinder final conclusions. Therefore, to address and confirm the *in vivo* interaction data, we sought to evaluate Ubc13-Mms2 binding properties *in vitro* by expressing and purifying each wild-type and mutant protein as GST fusions from

A



B

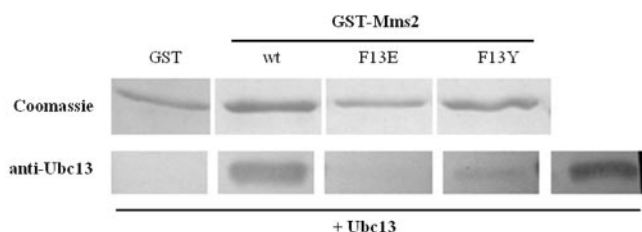


FIG. 4. *In vitro* binding of Ubc13 and Mms2 mutants. GST pull-downs were used to co-purify proteins that form stable interactions. A, purified GST-Ubc13 (wild-type or mutant) was immobilized. Cleaved Mms2 was then added, and after washing, the eluted GST-Ubc13 was visualized by Coomassie Blue staining, and Mms2 was detected by Western blot with antibodies against Mms2. B, experiment was performed as described in A, but with GST-Mms2 and cleaved Ubc13, and antibodies against Ubc13 were used for Western blot. The far right lane on each figure contains purified proteins as control.

bacteria and isolating the native non-fused protein when needed. Any post-translational modifications missing from bacterial expression were not a concern because previous *in vitro* binding and ubiquitination studies have been performed with recombinant protein from bacterial sources (17).

In addition to the wild-type proteins, two groups of mutants from each of Ubc13 and Mms2 were purified. These include those that resulted in reduced binding and functional complementation (Mms2-F13Y and Ubc13-R70A) and those that seemed to completely disrupt the interface and abolish function (Mms2-F13E and Ubc13-F57E). Despite rigorous attempts, GST-Ubc13-E55Q could not be expressed in soluble form in bacteria. To show that the lack of *in vivo* binding and function in this mutant was not due to insolubility in yeast cells, we tested the ability of Ubc13-E55Q and the other Ubc13 mutants to interact with TRAF6. The physical interaction between Ubc13 and TRAF6 has been demonstrated in the two-hybrid assay and is independent of Ubc13-Uev interaction (36). Therefore, the Glu⁵⁵ interface mutation is not expected to affect binding to TRAF6. Indeed, we were able to show that Ubc13-E55Q and the other Ubc13 mutants interact with TRAF6 with a strength that is indifferent to wild-type Ubc13.

We first used GST pull-downs (35) as a simple means to verify our *in vivo* interaction data. Purified wild-type or mutant GST-Ubc13 or GST-Mms2 was immobilized on glutathione-Sepharose and incubated with native Mms2 or Ubc13, respectively. Copurified proteins were then visualized by Western blot. Whereas Ubc13-F57E was unable to interact with Mms2, Ubc13-R70A retains binding ability (Fig. 4A). Similarly, Mms2-F13E apparently lost the ability to bind Ubc13, whereas Mms2-F13Y led to dramatically reduced binding with Ubc13 (Fig. 4B). These results are in agreement with the *in vivo* interaction data above (Fig. 2).

Surface Plasmon Resonance—Because *in vitro* pull-downs lack the quantitative capabilities for measuring binding strength, we employed SPR in order to more clearly show the effects of interface mutations on heterodimer formation. SPR

TABLE I
SPR binding data of Ubc13-Mms2 and their mutants

Ligand	Analyte	K_d^a	RU _{max}	Peak response at 1 μ M analyte
		<i>M</i>		<i>RU</i>
Ubc13	Mms2	1.87×10^{-7} , 1.07×10^{-7}	262	262
Ubc13	Mms2-F13A			15
Ubc13	Mms2-F13E			1
Ubc13	Mms2-F13Y			28
Mms2	Ubc13	6.22×10^{-8} , 5.14×10^{-8}	160	160
Mms2	Ubc13-F57E			6
Mms2	Ubc13-R70A			27

^a Calculated from curve-fitting and double reciprocal plots, respectively.

technology can be used to provide a sensitive real-time measure of protein-protein interactions, and the data may be used to determine kinetic and binding variables (37). In our experimental design, we used immobilized anti-GST monoclonal antibodies to capture the GST fusion protein (ligand), and the non-fused soluble binding partner (analyte) was subsequently applied to generate binding curves.

Because binding constants for the human Ubc13-Mms2 pair have been previously estimated using sedimentation (15) and NMR (18) analyses, we first sought to validate our SPR approach by determining the K_d for the wild-type Ubc13-Mms2 heterodimer. Using GST-Ubc13 fusions as the ligand, we were able to generate a series of curves over varied concentrations of native Mms2 as the analyte (supplemental Fig. S1, A). These curves were used in BiaEvaluation curve-fitting software to determine binding constants (Table I). We also generated our own double-reciprocal plots with the same data and found that our manually calculated dissociation constants were in close agreement (supplemental Fig. S2, A). To account for the possible effects of N-terminal GST fusions on binding strength, we performed the reciprocal approach using GST-Mms2 as the ligand and Ubc13 as the analyte (supplemental Figs. S1, B and S2, B). Notably, our binding constants for human Ubc13-Mms2 were found to be ~ 50 nM, which is in perfect agreement with those determined in independent isothermal titration calorimetry experiments (19).

Perhaps not surprisingly, we were unable to calculate meaningful binding constants for the Ubc13 and Mms2 mutations because in each case the binding was too weak to generate reliable data at the concentrations tested. Therefore, we tested each of the mutations against wild-type as a means of comparison. While using a constant concentration of analyte, we measured the peak response during binding at equilibrium (Table I). We would like to note that in order to better visualize the relative binding of mutant proteins, we had to use a concentration of analyte that was well above that which gave a maximum response for the wild-type proteins. Fig. 5 provides a good visual representation of the binding curves as compared with wild-type. From Fig. 5A and Table I, we can see that the Ubc13-F57E mutation results in barely detectable binding ($RU_{eq} = 6$). On the other hand, the maximum response of the Ubc13-R70A mutation was almost 5-fold higher ($RU_{eq} = 27$).

Through our studies above, it became apparent that the Mms2-Phe¹³ residue was a critical component to the interface. Therefore, to underscore the importance of Phe¹³, we chose to generate a third mutant at this position, Mms2-F13A. The F13A mutation corresponds to a yeast Mms2-F8A substitution that was created by another group (16), who suggested that it eliminates interaction and function with yeast Ubc13. Fig. 5B shows that each of the mutations at Phe¹³ results in considerably lower binding strength. Most strikingly, the introduction

A

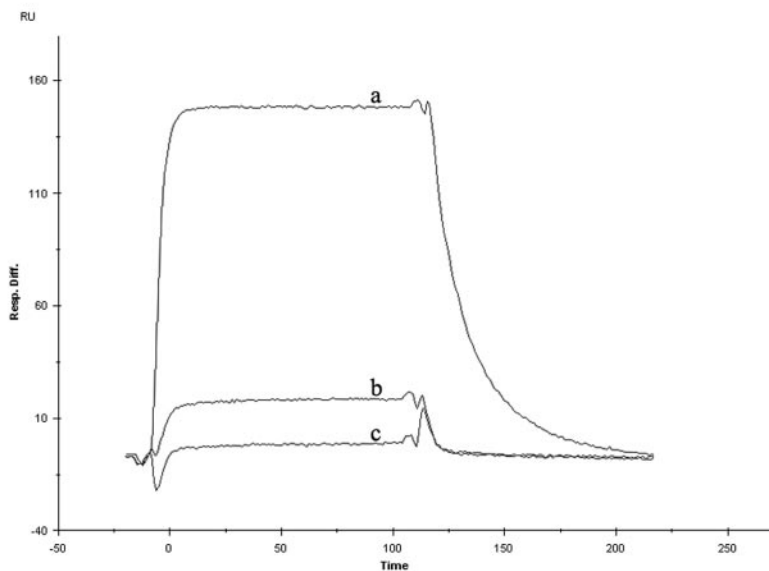
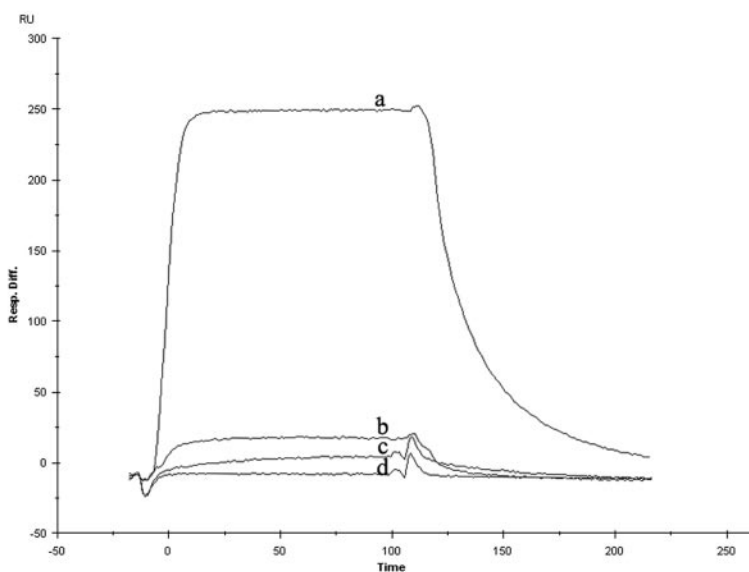


FIG. 5. Relative binding of Ubc13 and Mms2 mutants by SPR. *A*, relative binding of Ubc13 mutants to GST-Mms2. *a*, wild-type Ubc13; *b*, R70A; *c*, F57E. *B*, relative binding of Mms2 mutants to GST-Ubc13. *a*, wild-type Mms2; *b*, F13Y; *c*, F13A; *d*, F13E. Each experiment contains 1 μ M purified Ubc13 or Mms2 as the analyte. Note that maximum response for the wild-type protein interactions was also achieved when using 0.5 μ M protein.

B



of a charged group into the core of the interface via Mms2-F13E had the greatest effect on binding (Table I). The Mms2-F13E mutation resulted in peak binding that was barely detectable ($\text{RU}_{\text{eq}} = 1$), whereas the F13A mutation interaction was appreciably less weak ($\text{RU}_{\text{eq}} = 15$). Again, we find that the conservative introduction of small polar hydroxyl group through Mms2-F13Y leads to a lesser disruption of the Ubc13 interaction and binds nearly 2-fold stronger than F13A. Taken together, the SPR results are consistent with our initial observations for *in vivo* binding in the two-hybrid assay for both the Mms2 and Ubc13 mutants.

In Vitro Ubiquitination Assays—Because Lys⁶³ poly-Ub chains synthesized by Ubc13-Mms2 are required for DNA repair function, the *in vivo* functional complementation tests in Fig. 2 are a good indicator of Ub chain catalysis. However, we wished to provide a more direct test of Ub chain formation by

the mutant proteins. Therefore, we performed *in vitro* ubiquitination assays with purified components in which catalytic function is represented by the creation of di-Ub chains. Fig. 6 shows that wild-type Ubc13 and Mms2 form a strong band representative of di-Ub. In contrast, each of the mutations had a severe effect on di-Ub formation. In fact, neither Mms2-F13A, Mms2-F13E, Mms2-F13Y, nor Ubc13-F57E synthesized detectable Ub conjugates when paired with its wild-type partner. Only Ubc13-R70A led to observable di-Ub formation, which was much less than that observed for wild-type Ubc13. As previously reported (17), human Ubc13 has auto-Ub conjugation activity *in vitro*, and we observe that the interface mutations are not compromised in this regard.

Interactions between Ubc13-Arg⁷⁰ and Mms2-Phe¹³ Mutations—As discussed earlier, it was originally suggested that the Ubc13-Arg⁷⁰ residue might have a dual role with regard to the

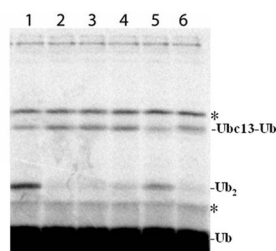


FIG. 6. Catalytic activity of Ubc13 and Mms2 mutants. Ubiquitination assays were performed to monitor di-Ub formation by the Ubc13-Mms2 complex. The autoradiogram shows radiolabeled Ub alone or conjugated Ub₂. The autocatalytic activity of Ubc13 is indicated, and asterisks reveal artifacts of the ³⁵S-labeled Ub (17). Lane 1, Ubc13 + Mms2; lane 2, Ubc13 + Mms2-F13A; lane 3, Ubc13 + Mms2-F13E; lane 4, Ubc13 + Mms2-F13Y; lane 5, Ubc13-R70A + Mms2; lane 6, Ubc13-F57E + Mms2. The Ub₂ bands that appeared in lanes 2, 3, and 6 are probably attributable to background signal because it was also seen in the absence of Mms2 (17).

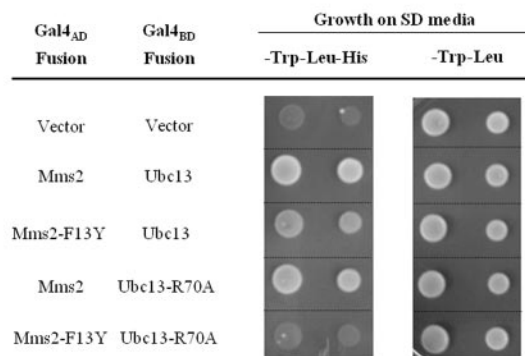
interface, namely, to share hydrophobic contacts with Mms2-Phe¹³ (Phe⁸ in yeast) and to form polar contacts with the Mms2 backbone via its guanidinium group. We reasoned that if the Ubc13-Arg⁷⁰-Mms2 backbone H-bond plays the dominant role, we would observe an additive effect on binding by mutations that remove the H-bond (Ubc13-R70A) and interfere with the hydrophobic contacts (Mms2-F13Y). The yeast two-hybrid assay (Fig. 7A) shows that whereas the combination of each of the mutants with its corresponding wild-type partner resulted in only slightly compromised binding, cells that carry both Ubc13-R70A and Mms2-F13Y mutations completely lost the interaction. The synergistic effect was also observed in a complementation experiment (Fig. 7B), in which yeast *mms2Δ ubc13Δ* cells co-transformed with *ubc13-R70A* and *mms2-F13Y* were no more resistant to MMS than the control cells, in contrast to cells carrying each single mutation.

Based upon the Ubc13-Mms2 crystal structure (Fig. 1B), we originally hypothesized that the Ubc13-R70A mutation would destroy any H-bonds but retain the contribution of hydrophobic contacts to the pocket. Therefore, the effect of the Ubc13-R70A mutation (Fig. 7, A and B) is suggestive of a second important interface contact point that is independent of the hydrophobic pocket. In order to better address this question, however, we generated a Ubc13-R70L mutant that would also abolish H-bonding but would be a better candidate for retaining hydrophobic contacts with Mms2-Phe¹³. As is seen in Fig. 7, the combination of Ubc13-R70A and Mms2-F13Y mutations completely abolished Ubc13-Mms2 interaction and DNA repair function in yeast cells, with phenotypes indistinguishable from the negative controls. In contrast, Ubc13-R70L did not demonstrate the same additive decrease in binding when coupled with Mms2-F13Y (Fig. 7C). In fact, the Ubc13-R70L mutation may have alleviated the affect of Mms2-F13Y. In addition, the Ubc13-R70L mutation was able to protect cells from MMS treatment as well as wild-type Ubc13 in functional complementation experiments (data not shown). Taken together, these results underscore the importance of Ubc13-Arg⁷⁰ in helping to create a deep Ubc13 hydrophobic pocket for Mms2-Phe¹³.

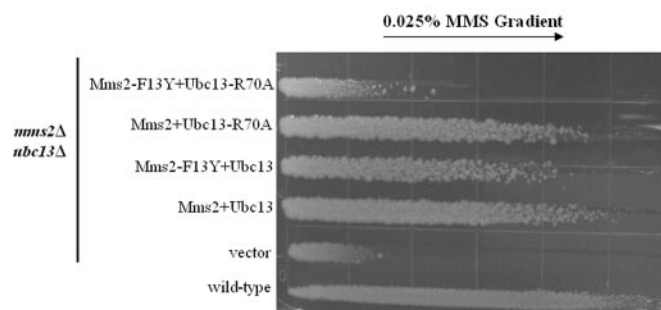
DISCUSSION

The Ubc13-Uev heterodimer is the only known E2 that creates atypical poly-Ub chains through Lys⁶³ *in vivo*. The uniqueness of the Ub-Uev complex in Ub chain synthesis led to numerous detailed biochemical studies (17–19) and the discovery of the involvement of Lys⁶³-linked Ub chains in various cellular pathways, especially in mammalian cells (1, 38–40). Importantly, mammals have two Uev proteins, Mms2 and Uev1, which have >90% sequence identity (26) but distinct

A



B



C

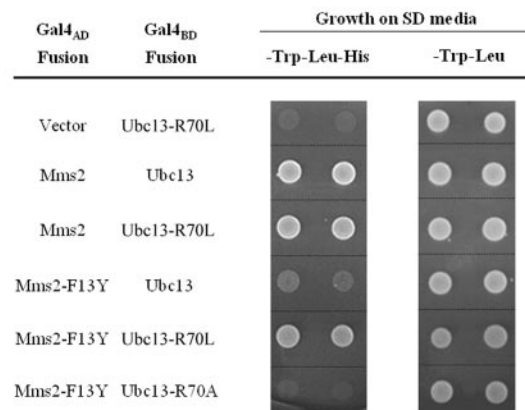


FIG. 7. Relationship between Ubc13-Arg⁷⁰ and Mms2-F13Y. The Mms2-F13Y and Ubc13-R70A or Ubc13-R70L mutations were co-transformed into yeast cells, and the double mutant was compared with wild-type and single mutants. A and C, the yeast two-hybrid assay to assess the strength of interaction between Gal4_{BD}-Ubc13-R70A and Gal4_{AD}-Mms2-F13Y and between Gal4_{BD}-Ubc13-R70L and Gal4_{AD}-Mms2-F13Y, respectively. Plates were incubated at 30 °C for 60 h in A and for 48 h in C. B, the gradient plate assay to assess heterologous complementation of yeast *mms2Δ ubc13Δ* mutant by human genes. Incubation was carried out for 48 h at 30 °C. All cells grew equally well on YPD plates without MMS (data not shown).

cellular functions;³ therefore, the formation of a particular Ubc13-Uev complex may serve as a means of regulation. However, whereas the mechanistic studies clearly describe how Ubc13-Uev complexes function, there is no report describing

³ P. L. Andersen and W. Xiao, unpublished data.

why the two proteins are able to come together to form a heterodimer. Prior to this investigation, there were only two interface mutations (Ubc13-E55A and Mms2-F8A) in yeast that were reported (16, 30). In this study, we made the first attempt to systematically mutate human Ubc13 and Mms2 in order to address how the complex is formed. We employed a number of *in vivo* and *in vitro* methods, including the yeast two-hybrid assay, pull-downs, and SPR in order to assess binding strength. In addition, an *in vitro* ubiquitination assay and a novel heterologous complementation approach were utilized to correlate binding ability with biochemical and biological activities. Overall, an excellent correlation between these experimental results was achieved.

The Ubc13-Mms2 interface is long and narrow and buries a large solvent-accessible surface area of ~ 1500 Å. Our study began with the systematic mutagenesis of a number of residues along the Loop 1, $\alpha 1$ helix, and the N terminus of Mms2, all of which contain portions that visibly contact Ubc13 in the human (15) (Fig. 1, A and B) and yeast (16) crystal structures. We ended up with the identification of a rather unexpected pocket of interactions close to the $\alpha 1$ helix of Mms2, which appears to be critical for both complex formation and specificity. This pocket consists of Phe⁵⁷ and Glu⁵⁵ of Ubc13 residing in close proximity to the N-terminal end of the Mms2 $\alpha 1$ helix believed to be the core of the Ubc13-Mms2 interface. Accordingly, both the Ubc13-F57E and Ubc13-E55Q mutations have extreme effects on disrupting the Ubc13-Mms2 interaction. In addition, Arg⁷⁰ can be viewed as a bridge between two Mms2 contact points because it putatively contributes hydrophobic contacts to the $\alpha 1$ helix of Mms2 (via Mms2-Phe¹³) and an H-bond with the Loop 1 backbone (via Mms2-Met⁴¹). Underlining its importance as another key interface residue, the Ubc13-R70A mutation compromised binding and function. Among residues in the Mms2 complement of the core interface region, the Mms2-N12D and Mms2-N12A mutations that disrupt the H-bond with Ubc13-Glu⁵⁵ did not have the same effect as the corresponding Ubc13-E55Q mutation. On the other hand, mutating Mms2-Phe¹³ had profound effects on binding and *in vivo* functions. Based on the Ubc13-Mms2 crystal structures, Mms2-Phe¹³ is seen to insert itself deep within a hydrophobic pocket formed by the Ubc13 backbone and several side chain carbons, reminiscent of a key in a keyhole. To fully explore the significance of this critical interaction, we created three very different mutations at this same Phe¹³ residue. An aggressive F13E mutation resulted in the complete loss of detectable binding in all of our *in vivo* and *in vitro* studies. To explore the importance of these hydrophobic contacts further and more precisely, we created and tested a more conservative mutation, F13Y. We found that the introduction of this small hydroxyl group was sufficient to severely disrupt the Ubc13-Mms2 interface, and this underscores the importance of the deep hydrophobic contacts required for the Phe¹³ insertion. Similarly, the Ubc13-Mms2 heterodimer is abrogated with an Mms2-F13A substitution that maintains the hydrophobic characteristic but cannot breach the Ubc13 surface to create deep hydrophobic contacts.

Whereas our studies have revealed a number of crucial Ubc13 interface residues, Mms2-Phe¹³ appears to be the only interface residue identified with a role in binding to Ubc13. A model based on crystal structures and this study suggests that Mms2-Phe¹³ is inserted between Ubc13-Glu⁵⁵ and Ubc13-Phe⁵⁷ and is flanked closely by Ubc13-Arg⁷⁰, which together form a critical hydrophobic interface pocket. This model is in agreement with the demonstrated stability of Ubc13-Mms2 salt concentrations as high as 2.5 M.⁴ It is thus likely that polar

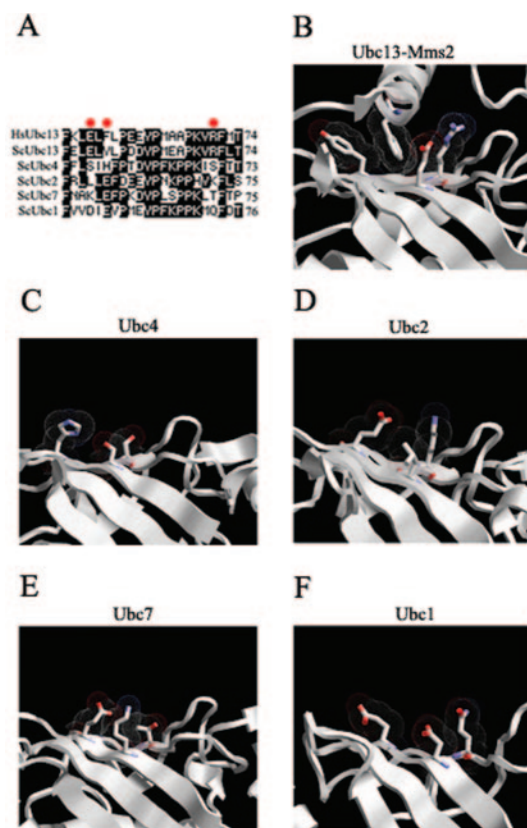


FIG. 8. A hydrophobic pocket is conserved in Ubc13 but not in other Ubcs. A, amino acid sequence alignment of yeast and human Ubc13 with yeast Ubc1, Ubc2/Rad6, Ubc4, and Ubc7. Residues corresponding to hUbc13-Glu⁵⁵, hUbc13-Phe⁵⁷, and hUbc13-Arg⁷⁰ are indicated. B–F, three-dimensional structure and comparison of various Ubcs highlighting residues corresponding to hUbc13-Glu⁵⁵, hUbc13-Phe⁵⁷, and hUbc13-Arg⁷⁰. B, interface of the yeast Ubc13-Mms2 crystal structure. C–F, other yeast Ubcs are presented in the same orientation as Ubc13. Visible residues are shown with Van der Waals forces and correspond to those found in this study to reside at critical positions in the human Ubc13-Mms2 complex. Images were generated using Ras-Top 2.0.3 by Philippe Valadon (www.geneinfinity.org/rastop/).

contacts, such as those observed in the crystal structures via the Ubc13-Arg⁷⁰ and Ubc13-Glu⁵⁵ residues, do not significantly contribute to binding strength and might instead play more subtle roles such as aiding Mms2-Ubc13 recognition.

Because of their functional interchangeability, the human (15) and yeast (16) crystal structures of the Ubc13-Mms2 heterodimers are very similar (26, 35). In particular, the corresponding interface residues that we mutated in the human proteins are conserved and oriented identically in yeast. A small caveat is the human Ubc13-Phe⁵⁷ residue, which corresponds to a Tyr⁵⁷ in yeast; however, Tyr⁵⁷ has its hydroxyl group pointed away from the critical hydrophobic pocket (supplemental Fig. S3). The above information allows us to use sequence alignments to determine the residues in other yeast Ubc structures (Fig. 8A) that correspond to human Ubc13-Glu⁵⁵, Ubc13-Phe⁵⁷, and Ubc13-Arg⁷⁰. The positions of these corresponding residues for each of Ubc2/Rad6 (29), Ubc4 (13), and Ubc7 (41) are physically oriented such that the necessary hydrophobic pocket for Mms2-Phe¹³ is not permitted (Fig. 8, B–E). Although Ubc1 (42) might spatially allow an Mms2-Phe¹³ insertion, the stoutness of its Asp and Gln residues at the Ubc13-Glu⁵⁵ and Ubc13-Arg⁷⁰ positions, respectively, would not allow sufficient hydrophobic contact from their side chains (Fig. 8F). It would be of great interest to see in future studies whether these critical Ubc13 residues are not only required but also sufficient to interact with Mms2.

⁴ L. Pastushok, unpublished results.

Acknowledgments—We thank Jing Hu for the kind gifts of Ubc13-L83A, Ubc13-Y34A, and Mms2-F13A mutant clones; Jason Maley for assistance in SPR experiments; and Michelle Hanna for critical reading of the manuscript.

REFERENCES

- Pickart, C. M. (2001) *Annu. Rev. Biochem.* **70**, 503–533
- Wei, W., Ayad, N. G., Wan, Y., Zhang, G. J., Kirschner, M. W., and Kaelin, W. G., Jr. (2004) *Nature* **428**, 194–198
- Zhang, H. G., Wang, J., Yang, X., Hsu, H. C., and Mountz, J. D. (2004) *Oncogene* **23**, 2009–2015
- Fisk, H. A., and Yaffe, M. P. (1999) *J. Cell Biol.* **145**, 1199–1208
- Kao, C. F., Hillyer, C., Tsukuda, T., Henry, K., Berger, S., and Osley, M. A. (2004) *Genes Dev.* **18**, 184–195
- Hochstrasser, M. (1996) *Annu. Rev. Genet.* **30**, 405–439
- Wu-Baer, F., Lagrazon, K., Yuan, W., and Baer, R. (2003) *J. Biol. Chem.* **278**, 34743–34746
- Arnason, T., and Ellison, M. J. (1994) *Mol. Cell. Biol.* **14**, 7876–7883
- Baboshina, O. V., and Haas, A. L. (1996) *J. Biol. Chem.* **271**, 2823–2831
- Spence, J., Gali, R. R., Dittmar, G., Sherman, F., Karin, M., and Finley, D. (2000) *Cell* **102**, 67–76
- Galan, J. M., and Haguenuer-Tsapis, R. (1997) *EMBO J.* **16**, 5847–5854
- Hofmann, R. M., and Pickart, C. M. (1999) *Cell* **96**, 645–653
- Cook, W. J., Jeffrey, L. C., Xu, Y., and Chau, V. (1993) *Biochemistry* **32**, 13809–13817
- Koonin, E. V., and Abagyan, R. A. (1997) *Nat. Genet.* **16**, 330–331
- Moraes, T. F., Edwards, R. A., McKenna, S., Pastushok, L., Xiao, W., Glover, J. N., and Ellison, M. J. (2001) *Nat. Struct. Biol.* **8**, 669–673
- VanDemark, A. P., Hofmann, R. M., Tsui, C., Pickart, C. M., and Wolberger, C. (2001) *Cell* **105**, 711–720
- McKenna, S., Spyrapoulos, L., Moraes, T., Pastushok, L., Ptak, C., Xiao, W., and Ellison, M. J. (2001) *J. Biol. Chem.* **276**, 40120–40126
- McKenna, S., Moraes, T., Pastushok, L., Ptak, C., Xiao, W., Spyrapoulos, L., and Ellison, M. J. (2003) *J. Biol. Chem.* **278**, 13151–13158
- McKenna, S., Hu, J., Moraes, T., Xiao, W., Ellison, M. J., and Spyrapoulos, L. (2003) *Biochemistry* **42**, 7922–7930
- Pastushok, L., and Xiao, W. (2004) *Adv. Protein Chem.* **69**, 279–306
- Rothstein, R. J. (1983) *Methods Enzymol.* **101**, 202–211
- Xiao, W., Chow, B. L., Fontanie, T., Ma, L., Bacchetti, S., Hryciw, T., and Broomfield, S. (1999) *Mutat. Res.* **435**, 1–11
- Brusky, J., Zhu, Y., and Xiao, W. (2000) *Curr. Genet.* **37**, 168–174
- Adames, A. G., Gottschling, D. E., Kaiser, C. A., and Stearns, T. (1997) *Methods in Yeast Genetics*, Cold Spring Harbor Laboratory Press, Cold Spring Harbor, NY, E.
- Ito, H., Fukuda, Y., Murata, K., and Kimura, A. (1983) *J. Bacteriol.* **153**, 163–168
- Xiao, W., Lin, S. L., Broomfield, S., Chow, B. L., and Wei, Y. F. (1998) *Nucleic Acids Res.* **26**, 3908–3914
- Ke, S. H., and Madison, E. L. (1997) *Nucleic Acids Res.* **25**, 3371–3372
- James, P., Halladay, J., and Craig, E. A. (1996) *Genetics* **144**, 1425–1436
- Worthylake, D. K., Prakash, S., Prakash, L., and Hill, C. P. (1998) *J. Biol. Chem.* **273**, 6271–6276
- Ulrich, H. D. (2003) *J. Biol. Chem.* **278**, 7051–7058
- Broomfield, S., Chow, B. L., and Xiao, W. (1998) *Proc. Natl. Acad. Sci. U. S. A.* **95**, 5678–5683
- Broomfield, S., Hryciw, T., and Xiao, W. (2001) *Mutat. Res.* **486**, 167–184
- Li, Z., Xiao, W., McCormick, J. J., and Maher, V. M. (2002) *Proc. Natl. Acad. Sci. U. S. A.* **99**, 4459–4464
- Franko, J., Ashley, C., and Xiao, W. (2001) *Biochim. Biophys. Acta* **1519**, 70–77
- Ashley, C., Pastushok, L., McKenna, S., Ellison, M. J., and Xiao, W. (2002) *Gene (Amst.)* **285**, 183–191
- Wooff, J., Pastushok, L., Hanna, M., Fu, Y., and Xiao, W. (2004) *FEBS Lett.* **566**, 229–233
- Szabo, A., Stolz, L., and Granzow, R. (1995) *Curr. Opin. Struct. Biol.* **5**, 699–705
- Bothos, J., Summers, M. K., Venere, M., Scolnick, D. M., and Halazonetis, T. D. (2003) *Oncogene* **22**, 7101–7107
- Zhou, H., Wertz, I., O'Rourke, K., Ultsch, M., Seshagiri, S., Eby, M., Xiao, W., and Dixit, V. M. (2004) *Nature* **427**, 167–171
- Wertz, I. E., O'Rourke, K. M., Zhou, H., Eby, M., Aravind, L., Seshagiri, S., Wu, P., Wiesmann, C., Baker, R., Boone, D. L., Ma, A., Koonin, E. V., and Dixit, V. M. (2004) *Nature* **430**, 694–699
- Cook, W. J., Martin, P. D., Edwards, B. F., Yamazaki, R. K., and Chau, V. (1997) *Biochemistry* **36**, 1621–1627
- Hamilton, K. S., Ellison, M. J., Barber, K. R., Williams, R. S., Huzil, J. T., McKenna, S., Ptak, C., Glover, M., and Shaw, G. S. (2001) *Structure (Camb.)* **9**, 897–904